Supporting Materials for

Surface engineering of SnO_2 for improved perovskite/SnO_2 photodetectors

Jing Cai[1], Guipeng Li[2], Yulong Ying[3], Hongping Li[4,*], Ahmad Fairuz Omar[1], Marzaini Rashid[1,*], Mingming Chen[2,*]

1 School of Physics, Universiti Sains Malaysia, 11800 USM, Penang, Malaysia.

2 Department of Microelectronics, Jiangsu University, Zhenjiang, Jiangsu 212013, China.

3 School of Materials Science and Engineering, Zhejiang Sci-Tech University, Hangzhou, 310018, China.

4 School of Materials Science and Engineering, Jiangsu University, Zhenjiang, Jiangsu 212013, China.

*Corresponding authors:

hpli@ujs.edu.cn (H. Li), marzaini@usm.my (M. Rashid), andychain@live.cn (M. Chen)

EXPERIMENTS

Materials. MAI (>99.9%), PbI_2 (99.999%), $CH_3COOC_2H_5$ (AR), dimethyl formamide (DMF, anhydrous), dimethyl sulfoxide (DMSO, anhydrous), SnO_2 aqueous solution (3.0 wt%), $(NH_4)_2WS_4$.

Surface engineering of SnO_2. The surface engineering of SnO_2 was performed as follows: $(NH_4)_2WS_4$ was added to the SnO_2 aqueous solution at concentrations of 1.0, 2.0, and 4.0 mg/mL, and the mixture was stirred at room temperature overnight. During stirring, the surface V_Os of SnO_2 were passivated through the S substitution.

Preparation of $MAPbI_3/SnO_2$ PDs. Indium tin oxide (ITO) substrates were cleaned with acetone, ethanol, and DI water. Then, the substrates were dried with N_2 and treated with O_2 plasma for 10 min. After that, $SnO_2/(NH_4)_2WS_4$ aqueous solution was spin-coated on ITO, followed by annealing at 150 °C to prepare SnO_2 thin films (labeled as S-SnO_2). Finally, the perovskite precursor, which was prepared by dissolving MAI, PbI_2 and ZIF-67 into DMF/DMSO mixtures, was spin-coated on S-SnO_2, followed by a two-step annealing process [1]. All experiments were carried out in an atmosphere with a humidity of ~ 50%. The scheme of preparation of $MAPbI_3$/S-SnO_2 heterojunctions is depicted in Fig. 1a in the main text. Patterned top Au electrodes were deposited using sputtering method with a metal mask. For comparison, $MAPbI_3/SnO_2$ heterojunctions were prepared under identical conditions, where the SnO_2 thin films were prepared with a pure SnO_2 aqueous solution (i.e., without surface engineering treatment).

Characterization. The morphology of SnO_2 and $MAPbI_3$ thin films was investigated by scanning electron microscopy (SEM, JSM-7800F). The structure of $MAPbI_3$ thin films was investigated by X-ray diffraction (XRD, Bruker D8 with Cu Ka radiation of 1.54 Å). The steady-state and transient photoluminescence (PL) spectra of $MAPbI_3$ thin films were characterized with a picoseconds (ps)-pulsed laser at 450 nm. The transient PL data were recorded by a ps time-correlated single photon counting technique. X-ray photoelectron spectroscopy (XPS) was performed to study the atomic electron binding energies of SnO_2 thin films. The performance of $MAPbI_3/SnO_2$ heterojunction PDs was characterized by a photoresponse characterization system consisting of a Xenon lamp,

an electronic shutter, an optical attenuator, a monochromator, a microscope, two probes, a Keithley 2401, and a semiconductor parameter analyzer (Keysight, B1500A). The light power of the Xenon lamp was obtained from a standard Si PD.

Density functional theory calculations. Density functional theory calculations were carried out within the Vienna ab initio simulation package. The generalized gradient approximation in the form of the Perdew-Burke-Ernzerhof (PBE) exchange-correlation functional (GGA-PBE) was employed. For the case of S doped SnO_2, SnO (110) surface with dimensions 9.73 × 13.58 $Å^2$ was constructed with 5 atom layers, in which 2 bottom layers were fixed at the optimized bulk positions. In each slab model, an adequately vacuum space of > 15 Å to eliminate possible interactions between neighboring slabs. Two types of vacancy configurations were constructed: i.e., (i) O vacancy: removal of a single O atom on the SnO (110) surface; (ii) S substituting for O: S atom occupies the site of the O defect. The k-point mesh for the Brillouin zone was set as 4×3×1. As for the $MAPbI_3$ system, four types of vacancy configurations were constructed within the 2×2×2 supercell: i.e., (i) I vacancy: removal of a single I atom in the stoichiometric host cell; (ii) Pb vacancy: removal of a single Pb atom in the stoichiometric host cell; (iii) S substituting for I: a S atom occupies one I site in the stoichiometric host cell; (iv) S substituting for I with a Pb vacancy nearby: a S atom occupies one I site with a nearest Pb vacancy in the stoichiometric host cell. The structure was fully relaxed when the energy of electron self-consistent iteration was less than $1.0×10^{-5}$ eV/atom and the interatomic forces were less than 0.02 eV/Å.

Reference

1. Lee, J. H.; Shin, D.; Rhee, R.; Yun, S.; Yeom, K. M.; Chun, D. H.; Lee, S.; Kim, D.; Yi, Y.; Noh, J. H.; Park, J. H., Band Alignment Engineering between Planar SnO_2 and Halide Perovskites via Two-Step Annealing. *J. Phys. Chem. Lett.* **2019,** *10* (21), 6545-6550.

Supporting Figures

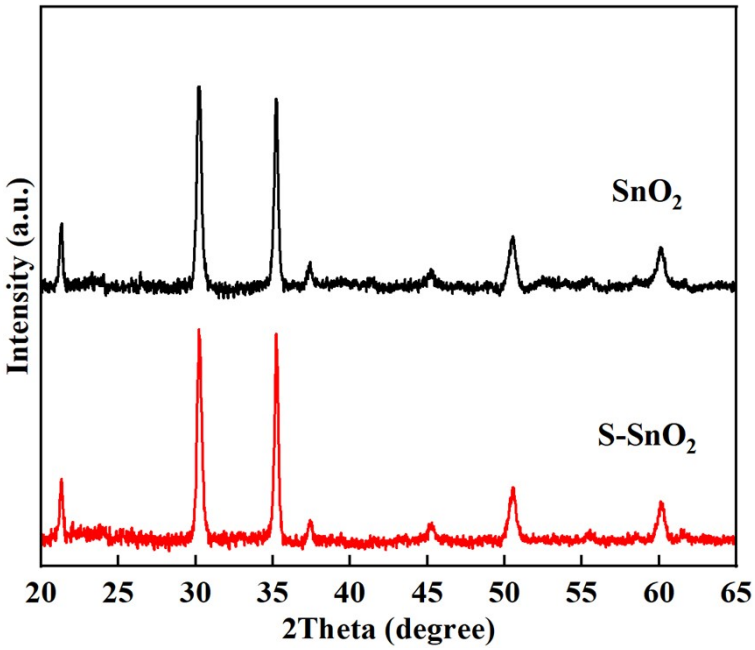

Fig. S1. XRD patterns of SnO_2 and S-SnO_2 thin films.

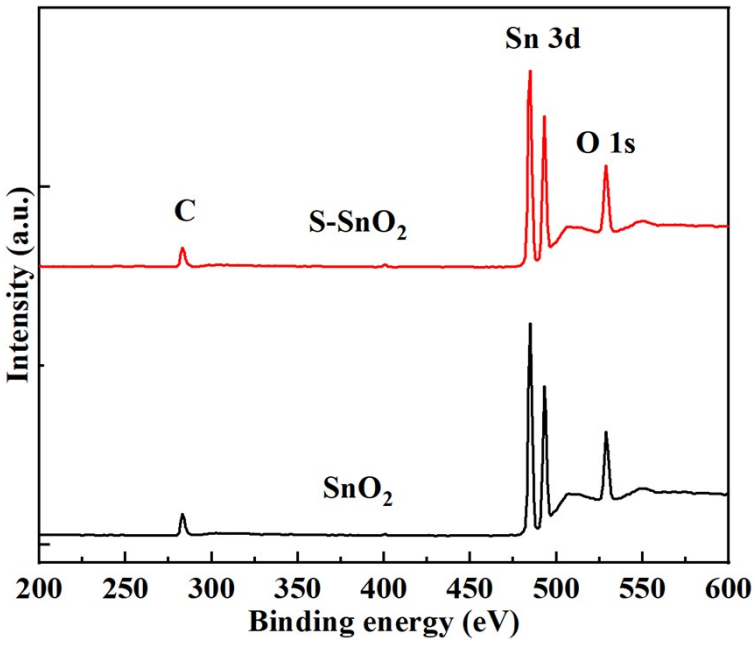

Fig. S2. XPS spectra of SnO_2 and S-SnO_2 thin films.

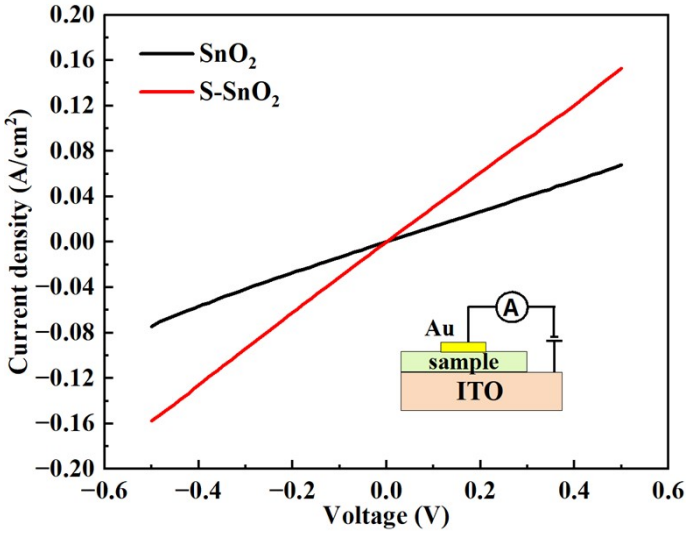

Fig. S3. I-V curves of Au/SnO_2/ITO and Au/S-SnO_2/ITO structures.

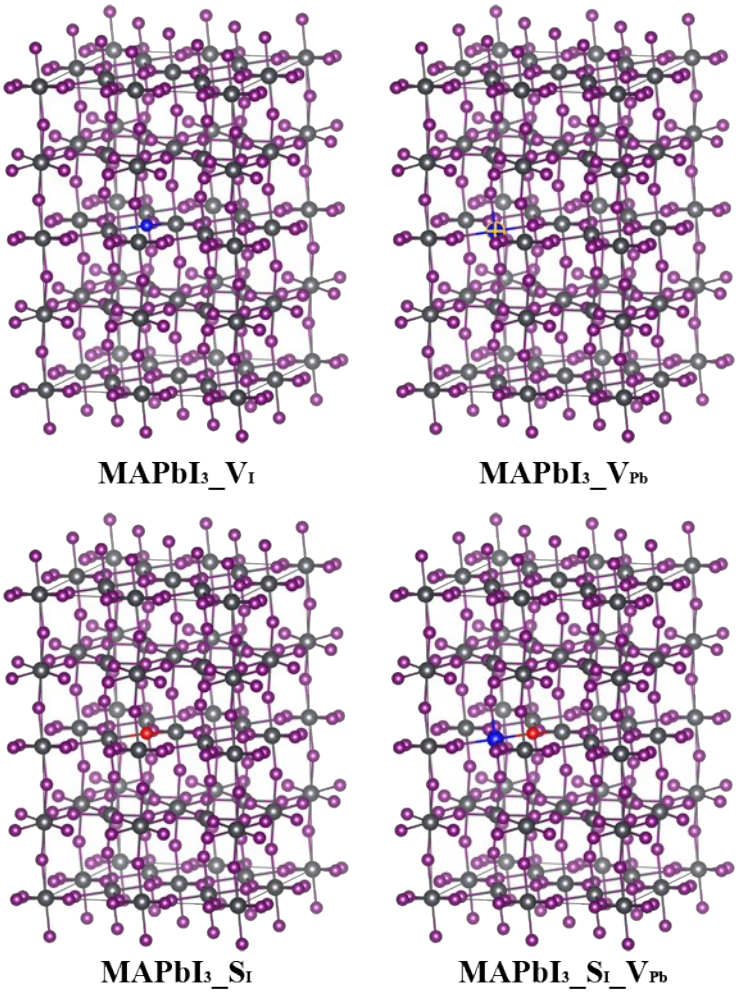

Fig. S4. Structures of $MAPbI_3$ supercells containing various defects. The vacancy and S substituting are labeled as blue and red spheres, respectively. The CH_3NH_3 groups are not shown herein.

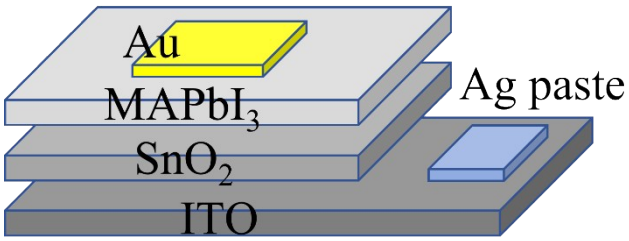

Fig. S5. Scheme of $MAPbI_3/SnO_2$ heterojunction PDs.

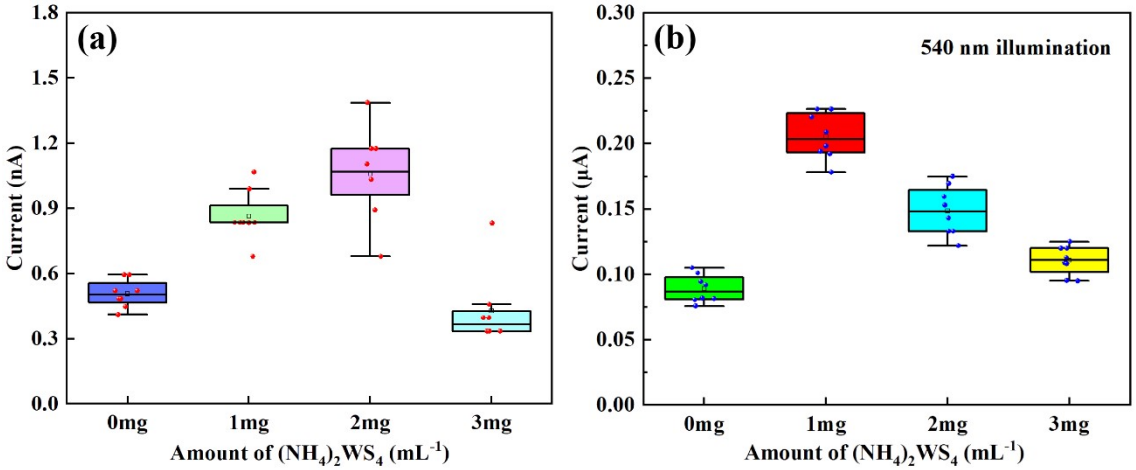

Fig. S6. Statistical results of dark current and photocurrent of $MAPbI_3/SnO_2$ PDs engineered with different concentrations of $(NH_4)_2WS_4$.

Supporting Tables

Table S1. Comparison of crystalline of $MAPbI_3$ thin films prepared on SnO_2 and S-SnO_2.

Crystalline plane	XRD peaks position (°)		FWHM (°)	
	On SnO_2	On S-SnO_2	On SnO_2	On S-SnO_2
020	14.16	14.16	0.0938	0.1223
002	20.06	20.06	0.1132	0.1156
031	23.54	23.54	0.1213	0.1423
220	24.56	24.54	0.1269	0.1484
040	28.50	28.48	0.1274	0.1503
230	30.26	30.30	0.3679	0.3287
141	31.94	31.92	0.1432	0.1511
321	35.26	35.24	0.3810	0.3553
400	40.72	40.70	0.1835	0.1822